J. Anat. (1993) 182, pp. 249–257 with 8 figures Printed in Great Britain

Morphometry of human thigh muscles. Determination of fascicle architecture by magnetic resonance imaging

S. H. SCOTT[1], C. M. ENGSTROM[2]* AND G. E. LOEB[1]

[1] *MRC Group in Sensory-Motor Physiology, Department of Physiology and* [2] *Department of Anatomy, Queen's University, Kingston, Ontario, Canada*

(*Accepted 14 January 1993*)

ABSTRACT

A previous investigation suggested that striation patterns spanning individual muscles in longitudinally oriented MR images may represent the orientation of its fascicles. In this study, we confirmed that these striation patterns could be used to infer fascicle orientation and to compute other architectural features of muscles from MR images. The volumes of 14 muscles within a cadaveric thigh were shown to be estimated accurately from cross-sectional MR images by comparison with direct measures from muscle mass. The angles of striations were measured at several positions within vastus medialis and semimembranosus from sagittal and frontal-plane MR images. Mathematical techniques were developed to infer the 3-dimensional orientation of fascicles based on these striation angles. The angle of striations in a 3rd oblique plane was shown to agree with mathematical predictions based on these computed orientations. The pennation angle, defined as the angle between the fascicles and the line of action of the muscle, predicted from the MR images, was similar to directly measured values. Interestingly, the pennation angle of these fascicles varied along the length of the muscle; in vastus medialis, pennation angle ranged from 5° to 50° in a proximodistal direction. Procedures were developed and validated to compute fascicle length by projection of fascicle orientation across the 3D shape of the muscles. The use of MR images to estimate muscle morphometry could improve greatly the predictive capabilities of musculoskeletal modelling by reducing the number of unknown model parameters.

INTRODUCTION

Musculoskeletal modelling has been used in many research fields as a tool for understanding movement (Seireg & Arvikar, 1973; Scott & Winter, 1990; He et al. 1991; Pandy & Zajac, 1991). However, even the simplest of these models contains many implicit and explicit parameters. Some of these describe the mechanical properties of muscle, while others describe the muscle's position and action on the skeletal system. As a result, analysis of the muscles spanning even a single joint generates an overwhelming number of unknown parameters that must be measured or estimated before the model can be used quantitatively.

Estimation of muscle morphometric parameters has traditionally relied on extrapolation from cadaveric specimens (Wickiewicz et al. 1983; Friederich & Brand, 1990). However, the large variability in the relative morphology of these muscles between specimens suggests that extrapolation to living subjects may be difficult (Friederich & Brand, 1990). In recent years, a variety of imaging techniques have been developed that allow visualisation of the structure of soft tissue in vivo (Ikai & Fukunaga, 1968; Maughan et al. 1983; Reid & Costigan, 1987). Engstrom et al. (1991) showed that with the high resolution provided by magnetic resonance (MR) images, individual thigh muscles can be clearly separated from surrounding tissues, permitting accurate determination of their cross-sectional area (CSA). In that study, striations spanning the widths of individual muscles were observed in longitudinal MR images of the lower limb

Correspondence to Dr G. E. Loeb, Biomedical Engineering Unit, Abramsky Hall, Queen's University, Kingston, Ontario, Canada, K7L 3N6.

* Present address: Department of Human Movement Studies, University of Queensland, St Lucia 4072, Australia.

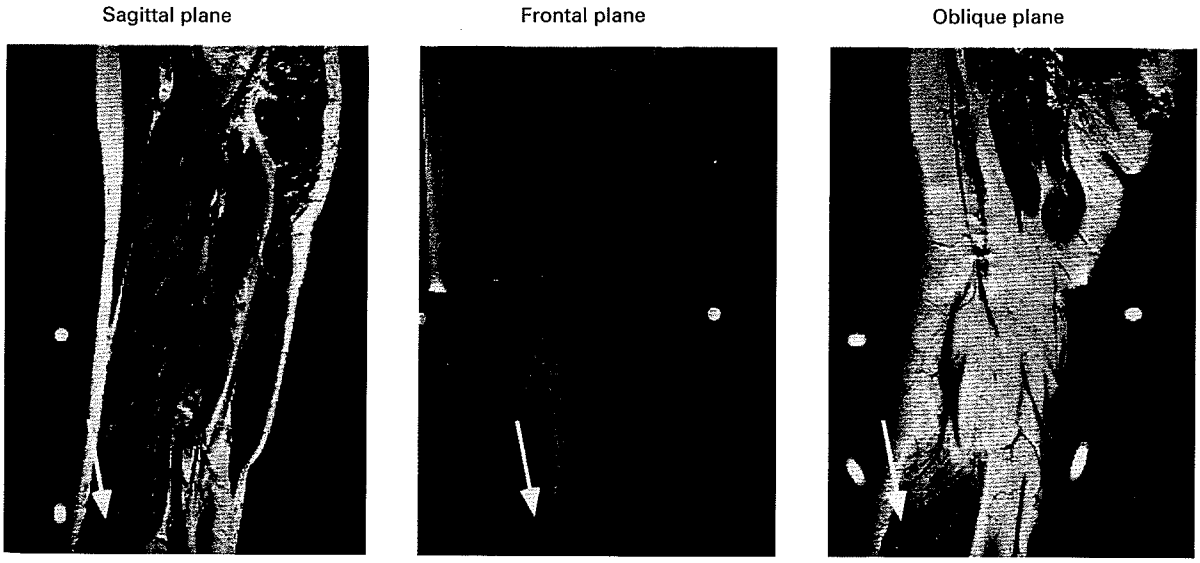

Fig. 1. Longitudinal MR images in the sagittal, frontal and an oblique plane (45° from frontal). The arrows identify a single point where a striation pattern is visible in all 3 planes.

(Fig. 1). These striations are generated by fat that runs parallel to and between the muscle fascicles (Engstrom et al. 1991). If the course of these striations represents a projection of the true fascicle orientation within the muscle, it should be possible to compute fascicle pennation angle and perhaps other related architectural parameters such as fascicle length and physiological cross-sectional area (PCSA). Such measurements in living subjects would allow muscle morphometric properties to be determined directly for each individual. This would reduce the number of estimated and extrapolated parameters contained in musculoskeletal models and would improve their predictive power.

In the present study, we used muscle striation patterns in MR images of cadaver lower limbs to infer the orientation of muscle fascicles in 3-dimensional (3D) space. Mathematical techniques were developed to compute the 3D orientation of fascicles from their projection in 2 orthogonal planes and to project these fascicles across the 3D shape of the muscle to estimate fascicle length and PCSA. The predictions from this analysis of MR images were compared with direct anatomical measurements in the same cadaver.

MATERIALS AND METHODS

The right lower limb of a male cadaver (death from cerebrovascular accident aged 79 y; mass 95 kg; height 1.8 m; fixed in ethanol-based preservative approximately 24 h after death) was prepared for MR imaging using previously described techniques (Engstrom et al. 1991). Briefly, the limb was mounted on a wooden frame to fix limb orientation. Reference tubes filled with a 5 mM copper sulphate solution were positioned on the frame to define and calibrate coordinates in the MR images. Standard soft-tissue MR (Siemens, 1.5 Tesla; TR, 700 ms; TE, 20 ms; NEX, 2) imaging protocols were used to generate serial, contiguous 10 mm cross-sections from the superior iliac crest to the knee joint (Engstrom et al. 1991). Longitudinal 5 mm sections at 5 mm intervals were taken in the frontal, sagittal and oblique (45° from frontal) planes. These longitudinal sections were centred midway between the hip and knee joints with a field of view of 35 cm. MR images were loaded onto a Macintosh IIx and displayed as a 256×256 matrix using image analysis software (Image, shareware from W. Rasband, NIMH).

Anatomical measurements

Subsequently, 14 of the muscles spanning the hip and/or the knee joints were excised and weighed. Measurements were taken on the muscle belly only, which included the muscle fascicles and the internal tendon. The volume of each muscle was estimated by dividing its mass by the density of skeletal muscle (1.06 g/ml; Méndez & Keys, 1960). Volume measures using Archimedes principle provided similar estimates, but larger variability between trials. Measurements of fascicle architecture were obtained from 2 muscles, vastus medialis and semimembranosus. The pennation angle, defined as the angle between the line of action of the muscle and the path of the fascicle (Gans, 1982), was measured using a goniometer at

different levels of each muscle. Individual fascicles were removed delicately from these muscles using blunt dissection and their lengths measured. PCSA has been defined in a variety of ways in the literature (see Friederich & Brand, 1990), but was computed here as muscle volume divided by fascicle length. These anatomical (AN) measurements were all performed before computing the MR results.

MR measurements

The volume of a muscle was calculated by multiplying the CSA of its profile in transverse MR images by the image interval (10 mm) and summing these values for all cross-sectional levels of the thigh. Measurement of the muscle CSA in each MR image followed our previously validated techniques (Engstrom et al. 1991). Muscle volumes were based on MR images that contained the muscle belly only, the fascicles and internal tendon (these are visible in the MR images), and not the external tendon. Individual structures were traced on photographic enlargements of the MR images. The perimeters of structures were traced manually with a stylus on a digitising tablet. The CSA of each structure was computed from these outlines using the MacMeasure software package (shareware from W. Rasband, NIMH) on the Macintosh IIx computer. Alternatively, point counting can be used to estimate CSA when automatic digitising systems are not available (see Gundersen & Jensen, 1987).

The muscle volumes were based upon 50 MR images of the limb. We estimated the error in the muscle volumes when using these 50 MR images, as well as the error when fewer images were sampled. The coefficient of error (CE), an estimate of the efficiency of the sampling procedure, was calculated when 6, 8, 10, 12, 16, 25 and 50 MR images were used to estimate the muscle volumes (Gundersen & Jensen, 1987; Mayhew & Olsen, 1991). These numbers correspond to systematic sampling of 1/8, 1/6, 1/5, 1/4, 1/3, 1/2 and 1/1 from the 50 MR images. The measurement of MR images in each sample followed the Cavalieri technique for volume estimation (Gundersen & Jensen, 1987; Mayhew & Olsen, 1991). However, since a uniform random seed was not used for the selection of the first section in each set, the samples do not qualify as generally valid Cavalieri samples (Gundersen & Jensen, 1987). Instead, the first image for the 1/n sampling procedure was the n/2 section in the 50 MR images. This approach centred the sampled MR images used for each sampling procedure midway between the superior iliac crest and the knee. Note that all of the muscles will not be visualised in all MR images. However, the selection of MR images spaced at regular intervals spanning the entire limb segment approximates more closely the selection of MR images that would be chosen when estimating the volumes of these limb muscles.

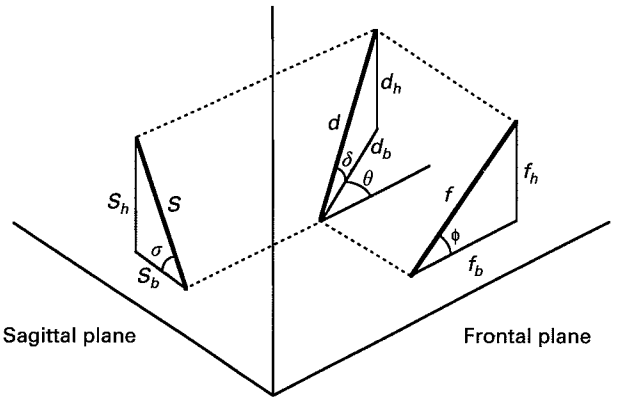

Fig. 2. A fascicle with length d has 2 orientation angles δ and θ. Its projection in the frontal and sagittal plane have lengths equal to f and s, respectively. The angle of the 2 projections, ϕ and σ, can be used to predict the orientation of the fascicle based on the equations in the text.

The 3D orientation of a fascicle within a muscle was predicted mathematically from its projection in the frontal and sagittal planes. The orientation of a fascicle with length d was described by 2 angles: δ, the fascicle angle relative to the horizontal plane and θ, the fascicle angle relative to the frontal plane (Fig. 2). The angle of its projection in the frontal and sagittal planes relative to the horizontal plane equalled ϕ and σ, respectively. The orientation of the fascicle was solved (see Appendix A) from the 2 projection angles using

$$\delta = \tan^{-1}\left(\sqrt{\frac{\tan^2\sigma\tan^2\phi}{\tan^2\sigma+\tan^2\phi}}\right) \quad (1)$$

and

$$\theta = \sin^{-1}\left(\frac{\tan\delta}{\tan\sigma}\right). \quad (2)$$

Thus it is possible to calculate the actual 3D orientation of a fascicle if the muscle striations observed in the longitudinal MR images represent the fascicle projection.

To validate that the striations represent a projection of the fascicles, the measured angle of the striations in a 3rd projection plane was compared with the value predicted mathematically using the striation angles in the frontal and sagittal planes. Consider a 3rd projection plane, also perpendicular to the horizontal plane, at an angle β from the frontal plane. The

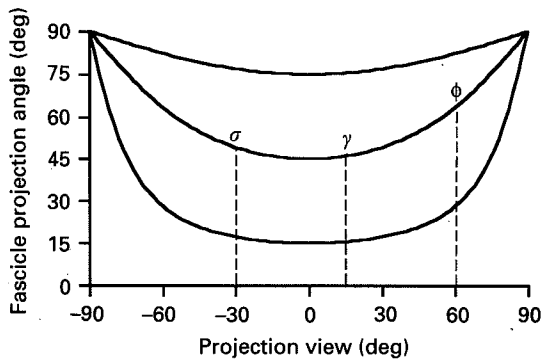

Fig. 3. The magnitude of the fascicle projection angle is dependent on the orientation of the fascicle. If the projection view is in line with the fascicle (projection view = 0°), the fascicle projection angle equals the fascicle orientation angle δ. As the projection view increases, the fascicle projection angle increases towards 90°. For the fascicle orientation angles δ = 45° and θ = 60°, the projection angles, ϕ, σ and γ equal 63°, 49° and 46°, respectively.

projection of the fascicle in this oblique plane has an angle γ from the horizontal plane and is solved using

$$\gamma = \tan^{-1}\left(\frac{\tan\delta}{\cos(\theta-\beta)}\right). \quad (3)$$

Therefore, if the striations in the frontal and sagittal MR images represent the projections of the fascicle orientation, the angle of the striations in the oblique plane should equal γ.

The relationship between the magnitude of the fascicle orientation angle, δ, and the magnitude of the projection angles, σ, ϕ and γ is illustrated in Figure 3 for 3 angles of δ. If the fascicle is oriented in the projection plane (projection view = 0°), the fascicle projection angle equals the fascicle orientation angle δ. As the projection plane becomes more out-of-plane from the fascicle (projection view increases or decreases), the fascicle projection angle becomes larger than the fascicle orientation angle δ. It would be expected gradually to become less distinct in the images, which represent averages over a finite thickness. Figure 3 also illustrates the relationship between the projection angles in the 3 projection planes when δ and θ equal 45° and 60°, respectively. In this case, the projection angles σ, ϕ and γ, are expected to equal 49°, 63° and 46°, respectively.

Several steps were required to estimate and validate fascicle orientation from the MR images. First, banding patterns were required to be visible for a given point within the muscle in all 3 planes: sagittal, frontal and oblique. This required an iterative approach to determine useable locations. The angle of striations in the frontal or sagittal plane was estimated by calculating the slope of a line drawn parallel to the banding pattern using tools provided by the Image software package. A 3D coordinate, P, on the striation was recorded. The MR image in the other plane (sagittal or frontal) that also contained point P was visualised and the slope of the striations at point P was measured. The 3D fascicle orientation was defined from the striation angles in the sagittal and frontal planes using equations 1 and 2. Finally, the striation angle in the oblique plane was predicted at point P and compared with the estimated angle based on equation 3.

The angles δ and θ describe the fascicle orientation in MR image coordinates and do not provide a direct measure of the fibre pennation angle in the muscle. Pennation angle, α, is defined as the angle between the fascicle orientation and the line of action of the muscle (Gans, 1982). The line of action of the muscle was determined from the positions of the tendon or aponeurosis in 2 cross-sectional MR images. The direction cosines, the angles between an object and each of the 3 coordinate axes, were calculated for both the fascicle and the muscle line of action. The angle of pennation was taken to be the angle between them:

$$\alpha = l_d l_a + m_d m_a + n_d n_a \quad (4)$$

where l_d, m_d and n_d were the direction cosines for the fascicle and l_a, m_a and n_a were the direction cosines for the line of action of the muscle relative to the x, y and z axes, respectively.

Fascicle length was estimated from the MR images using 2 different techniques. The first method assumed that the size and orientation of the CSA of the muscle remained constant in all MR images (Method 1) so that only one cross-section that contained point P was used in the analysis (Fig. 4). Fascicle length was assumed to equal the distance across the muscle that passed through point P at an angle θ divided by the cosine of δ.

A second method to estimate fascicle length followed the position of the fascicle through each cross-section (Method 2). Starting from the MR image that contained point P, sequential cross-sections, superior and inferior, were viewed and the position of the fascicle was marked based on its orientation angles, θ and δ. The distance between the 2 locations where the fascicle intersected the edges of the muscle defined fascicle length.

The PCSA reflects the number of muscle fibres acting in parallel within a muscle: the larger the PCSA, the greater the force generating capabilities of the muscle. Its value was estimated by dividing the volume of each muscle by its average fascicle length, as computed above from the MR images, and was

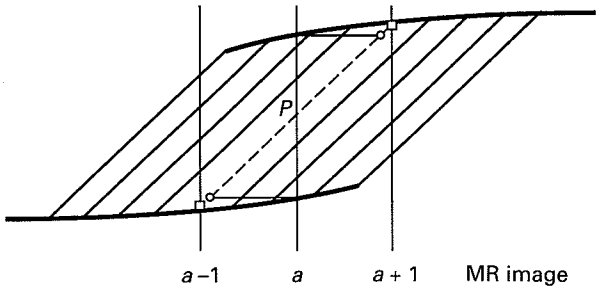

Fig. 4. The length of a fascicle was calculated in 2 different ways using the MR images. Method 1 assumed that fascicle length equalled the distance across the muscle that passed through point P at an angle θ, divided by the cosine of δ. This is equivalent to assuming that the 3D form of the muscle is a simple extrusion of its horizontal cross-section at the level containing point *P*. Method 2 followed the path of the fascicle through successive MR images, based on δ and θ, until the fascicle intersected the edge of the muscle; fascicle length was assumed to equal the distance between these intersections.

compared with the value calculated from the direct anatomical measurements for each muscle.

Table 1. *Comparison of muscle volumes based on muscle mass and MR images*

Muscle	Abbreviation	Vol. (mass) (cm^3)	Vol. (MRI) (cm^3)	Error (%)
Sartorius	Sr	158	158	0
Gracilis	Gr	83	75	−10
Semitendinosus	St	105	94	−10
Semimembranosus	Sm	177	167	−6
Biceps femoris (long head)	Bfl	153	138	−10
Biceps femoris (short head)	Bfs	79	78	−1
Adductor magnus	Am	525	489	−7
Adductor longus	Al	101	87	−14
Adductor brevis	Ab	68	110	62
Vastus medialis	Vm	358	379	6
Vastus intermedius	Vi	317	326	3
Vastus lateralis	Vl	468	478	2
Rectus femoris	Rf	141	135	−5
Tensor fasciae latae	Tfl	54	47	−12
Total		2788	2761	−1.0

RESULTS

Muscle volume

Fifty MR cross-sections of the limb spaced at 10 mm intervals were sampled to calculate the volume of individual muscles within the thigh. There was a good correspondence between muscle volumes estimated from the digitised MR images and those computed from muscle mass (Fig. 5 and Table 1). The estimates from MR images were mostly within 10% of those based on muscle mass. A large error in volume was found for the small adductor brevis muscle and was probably due to the difficulty in differentiating this structure in the MR cross-sections from adductor magnus (see Engstrom et al. 1991). The volume of most small muscles was underestimated slightly using MR images, but the total volume of all the muscles was almost identical to direct measures. When ambiguity over recognition of individual adductor muscles is removed by grouping them together (magnus plus longus plus brevis), the error term is reduced to less than 1%.

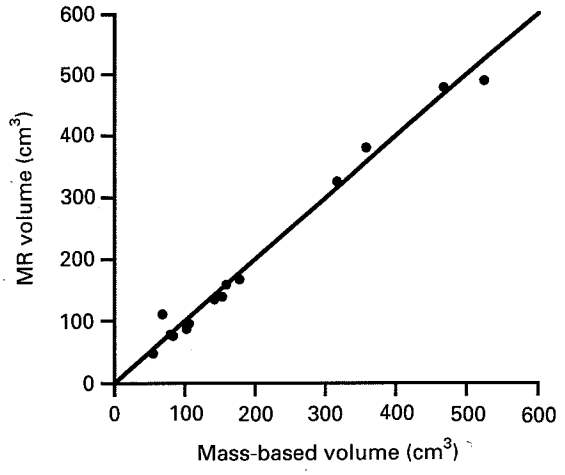

Fig. 5. Scatter plot of volumes estimated from muscle mass and MR images. Solid line denotes 45° line (perfect agreement).

The percentage CE in the muscle volume estimates were all below 5% when 50 MR images were sampled (Fig. 6 and Table 2). In general, the variation in the expected sampling error (the square of the CE) was inversely proportional to the number of samples that was used to estimate the volume of each muscle (see fig. 4 in Mayhew & Olsen, 1991). However, the CE rose more rapidly for some of the smaller, shorter muscles when fewer MR images of the limb were sampled because these muscles were visible in only a few MR images (see Table 2). For example, adductor brevis was visible in only 3 of the 12 MR images sampled, resulting in a percentage CE of 15.5.

Fascicle orientation

The angle of the muscle striations measured in the oblique-plane MR images was similar to the angle predicted mathematically from the striations in the frontal and sagittal plane images (Fig. 7). In vastus

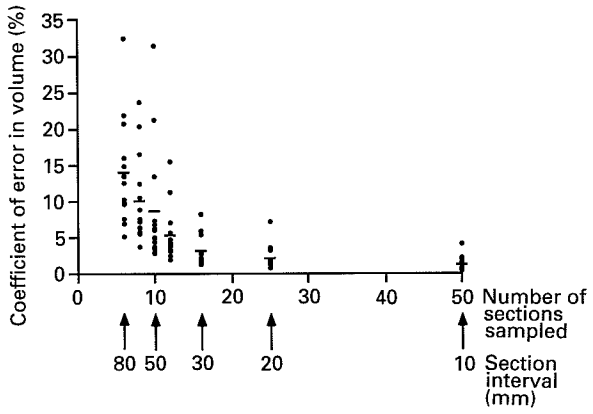

Fig. 6. The mean percentage CE, an estimate of the efficiency of the sampling procedure, for the muscle volumes was above 5% when 12 or fewer MR sections were sampled. Filled circles denote individual errors for each muscle, while the horizontal bar denotes the average for all muscles.

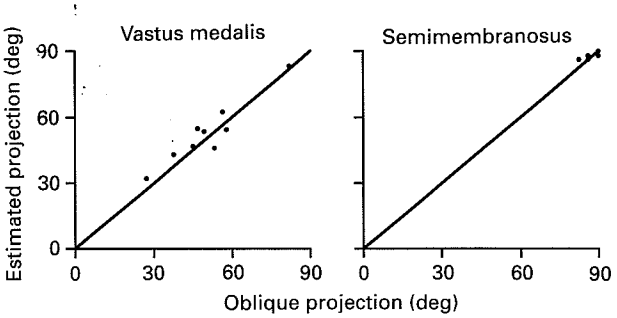

Fig. 7. Scatter plots of oblique projection angle and its estimate, based on frontal and sagittal projection angles. Solid line denotes 45° line (perfect agreement).

medialis, there was a good correlation between the measured and predicted oblique-plane striation angles. In semimembranosus, the consistent orien-

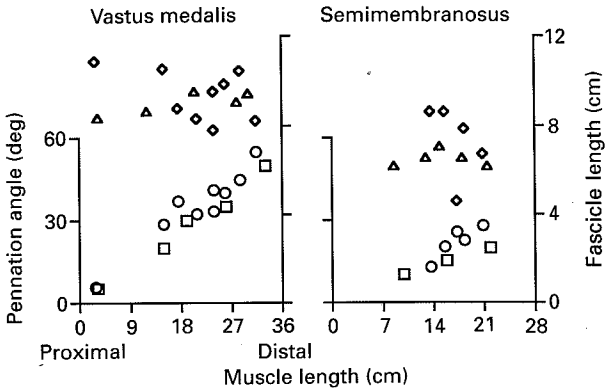

Fig. 8. Similar estimates of pennation angle and fascicle length were obtained from anatomical or MR estimates. Pennation angle increases in magnitude in a proximodistal direction within each muscle. Fascicle length remained relatively constant throughout each muscle. Only the second method for estimating fascicle length from MR images is shown. Diamonds, MR fascicle length; triangles, AN fascicle length; circles, MR pennation angle; squares, AN pennation angle.

tation of the fascicles in the MR images (i.e. θ remained consistent) resulted in a small range of fascicle projection angles in the oblique angle. In addition, fascicle orientation in this muscle was nearly perpendicular to the oblique plane, resulting in poor resolution of the muscle striations.

Pennation angles measured from the MR images were quite similar to the angles measured during dissection of each muscle (Fig. 8). There was a tendency for the angles predicted using the MR images to be slightly higher than direct measures. However, the limited accuracy of the intrusive, dissection measurements may be as much responsible for the discrepancy as the values obtained from MR

Table 2. *Percentage CE for each muscle based on the number of MR images sampled*

MR images	50	25	16	12	10	8	6
Muscle*	% CE (n)**	% CE (n)	% CE (n)	% CE (n)	% CE (n)	% CE (n)	% CE (n)
Sr	0.4 (50)	0.8 (25)	1.3 (16)	2.0 (12)	3.0 (10)	3.8 (8)	5.1 (6)
Gr	0.7 (31)	1.9 (16)	2.1 (11)	3.8 (8)	3.4 (7)	7.5 (5)	12.6 (4)
Sm	0.6 (26)	1.8 (13)	2.2 (9)	4.3 (7)	6.3 (5)	8.8 (5)	14.8 (3)
St	1.0 (29)	1.6 (15)	2.8 (10)	4.0 (7)	5.0 (6)	7.2 (5)	13.4 (3)
Bfs	1.0 (22)	1.9 (11)	3.0 (7)	5.6 (5)	6.8 (4)	12.5 (3)	13.6 (3)
Bfl	0.5 (15)	1.3 (12)	2.7 (8)	4.8 (6)	7.3 (5)	10.5 (4)	16.0 (3)
Am	1.6 (30)	1.6 (15)	2.1 (10)	3.4 (8)	6.0 (6)	5.7 (5)	10.2 (4)
Al	2.1 (17)	3.6 (8)	5.4 (6)	7.0 (5)	13.5 (3)	16.6 (3)	21.9 (3)
Ab	4.1 (13)	7.2 (6)	5.9 (5)	15.5 (3)	31.4 (2)	21.7 (2)	32.4 (2)
Vm	0.4 (37)	0.8 (19)	1.7 (12)	3.1 (9)	3.7 (7)	6.4 (6)	6.9 (5)
Vi	0.8 (34)	1.3 (17)	2.6 (12)	3.7 (9)	4.8 (7)	5.5 (6)	9.7 (5)
Vl	0.5 (36)	1.2 (18)	2.1 (12)	3.2 (9)	2.8 (7)	5.6 (6)	7.5 (4)
Rf	0.5 (31)	1.2 (15)	1.5 (10)	2.5 (8)	4.4 (6)	6.3 (5)	9.9 (4)
Tfl	1.9 (14)	3.2 (7)	8.2 (4)	11.2 (3)	21.2 (2)	20.4 (2)	20.7 (2)

* Key to abbreviations is given in Table 1.

** The number in parentheses denotes the actual number of MR images in which the muscle was visible. Note that many muscles were visible in only a small fraction of the MR images sampled.

Table 3. *Estimates of fascicle length and PCSA based on AN and MR images*

	Fascicle (cm±S.D.)	n	Error (%)	PCSA (cm^2)	Error (%)
Vastus medialis					
AN	8.97±0.46	6	—	38.9	—
MR					
Method 1	9.01±2.04	9	0	42.1	8
Method 2	9.42±1.15	9	5	40.2	3
Semimembranosus					
AN	6.44±0.37	5	—	27.4	—
ME					
Method 1	8.16±4.31	5	27	20.5	−25
Method 2	7.29±1.69	5	13	22.9	−17

images. Interestingly, the pennation angle varied considerably along the length of each muscle. Vastus medialis showed a particularly large variation in pennation angle, from only 5° at its most proximal end to 50° at its most distal end. Both the MR estimates and the directly measured values showed similar gradual increases in pennation between these 2 extremes. Semimembranosus demonstrated a smaller range of pennation angles: from 10° at the proximal end to 20° at its distal end.

Anatomical dissection of vastus medialis and semimembranosus revealed a constant fascicle length despite the gradients in angle of pennation (Fig. 8). Estimates of fascicle length from MR images were more precise using method 2, where the path of the fascicle was followed through successive MR cross-sectional images to its connective tissue attachments (Table 3). There was greater variability in fascicle length when its value was predicted from a single MR cross-section (Method 1).

Both MR methods accurately predicted the PCSA of vastus medialis, but the estimates were slightly low for semimembranosus (Table 3). The discrepancy in semimembranosus appears to be related to the multiplicative effects of underestimating the muscle volume and overestimating the fascicle lengths in the MR data.

DISCUSSION

We have shown empirically that it is possible to calculate values for fascicle orientation, length and pennation angle and muscle volume from MR images. Together, these values permit direct computation of most of the morphometric parameters used to quantify muscle architecture in models of force production by muscles. Previous studies have shown that MR images can be used to estimate the moment arms of muscles in vivo (Rugg et al. 1990; Spoor & Van Leeuwen, 1992). Our results add to the potential role of MR imaging in quantifying the properties of the musculoskeletal system. This would be valuable for researchers developing biomechanical models of the human body as well as those studying morphological adaptations of the musculature in humans under a variety of conditions.

Improvements to the methods

Although the morphometric properties of muscle could be determined from MR images, the techniques presented could be improved. To begin, considerable knowledge of the gross anatomical organisation of each muscle as well as its representation in the MR images is required by the investigator in order to make informed but subjective decisions about muscle boundaries (Engstrom et al. 1991). In addition, manual calculations are now necessary to select iteratively those MR images that correspond to similar positions within a muscle in different planar views. An interactive computer software environment that incorporated automatic registration of images from multiple views would improve operator efficiency.

A reduction in the number of MR images used to estimate the volume of each muscle would reduce the time to compute muscle volumes. As shown in Table 2, the number of MR images sampled within a limb segment can be much larger than the number of images that contain cross-sections of individual muscles. The selection of an appropriate range and spacing of images requires prior estimation of the anatomical extent of the muscles under study.

The techniques employed to calculate the architectural parameters may not be appropriate for all muscles and may require modifications for muscles of varying architecture. For example, the measurement of fascicle length assumed that each fascicle followed a straight line between its connective tissue attachments. However, the sartorius muscle follows a long and slightly circuitous route from its origin on the iliac crest to its insertion on the medial side of the tibia. Alternatively, a better measure of its fascicle length would be based upon the coordinates of its centroid in transverse MR images. An interactive computer package would again prove valuable for such calculations.

Muscle striations were not visible in all muscles in longitudinal images of the thigh. These patterns, probably generated by fat running parallel with the fibres, will be dependent on many factors in addition to the muscles' fat content. First, the value of each

pixel in the MR image represents the average signal intensity generated from a cube of tissue 1.4 mm × 1.4 mm × 5 mm. An enhancement of the muscle striations may be possible if the size of this voxel is reduced, that is, improving the spatial resolution of the images by reducing the image thickness below 5 mm (used in this study), by increasing the magnification of the muscle in the MR image, or by using a larger bitmap (256 × 256 used in this study). Secondly, striations were resolved most clearly in MR images that were coplanar with the fascicle orientation and were hard to distinguish when the views were nearly orthogonal to the fascicles. This poses a significant problem if all muscles spanning a joint are to be characterised because fascicle orientation will be different for each muscle and may even change along the course of each muscle. In this study, analysis of fascicle orientation was based upon 2 orthogonal images of the thigh, oriented in the sagittal and frontal planes. An alternative approach would be to analyse the striation patterns in longitudinal MR images oriented in the sagittal, frontal and one or more oblique planes. The orientation of the fascicle could then be computed from a weighted combination of the projection angles of the fascicle in all views that contained striation patterns for a given point in the muscle. Preferably, facilities that use volume scans could use image reformatting to align an image in the plane of the fascicles in each muscle, but this would require very high voxel resolution. Such images would permit direct measurement of fascicle length; angle of pennation would still have to be computed from the angular difference between the fascicle and the line of pull of the muscle.

The consequences of variable pennation angles in vastus medialis

The large variation in pennation angle in vastus medialis means that incremental changes in whole-muscle length will not be transmitted uniformly to all fascicles. In a simple planimetric representation of muscle, fascicles nearly parallel to the line of action of the tendon match whole-muscle excursion, whereas highly pennate fibres rotate so that their length changes by only a fraction of whole-muscle excursion (Gans, 1982; Scott & Winter, 1991). Therefore, even if all the fascicles have the same length and sarcomere spacing under some initial condition, changes in overall muscle length will result in different relative length changes in different regions of the muscle, although the actual values will also depend on other factors such as compliance in the aponeurotic sheets (Ettema & Huijing, 1990). Most simple models of muscle assume a single angle of pennation for the entire muscle. Simply assuming a single effective angle of pennation for all fascicles may not be adequate for representing muscles with as large a range of pennation angles as vastus medialis (0–50°). Perhaps the mechanics of these muscles may only be determined either by direct measurements, which are not presently possible in humans, or through complex models of muscle that incorporate factors such as variable pennation angle, fascicle length and aponeurotic compliance (Woittiez et al. 1984; Otten, 1988).

ACKNOWLEDGEMENTS

This work was supported by a grant from the Muscular Dystrophy Association of Canada. We thank Dr L. Avruch for assistance with collection of the MR images and Mr R. Hunt for assistance in the anatomical work.

REFERENCES

Engstrom CM, Loeb GE, Reid JG, Forrest WJ, Avruch L (1991) Morphometry of the human thigh muscles. A comparison between anatomical sections and computer tomography and magnetic resonance imaging. *Journal of Anatomy* **176**, 139–156.

Ettema GJC, Huijing PA (1990) Architecture and elastic properties of the series elastic element of muscle-tendon complex. In *Multiple Muscle Systems: Biomechanics and Movement Organization* (ed. J. M. Winters & S. L-Y. Woo). New York: Springer.

Friederich JA, Brand RA (1990) Technical note: muscle fiber architecture in the human lower limb. *Journal of Biomechanics* **23**, 91–95.

Gans C (1982) Fiber architecture and muscle function. *Exercise and Sport Sciences Reviews* **10**, 160–207.

Gundersen HJG, Jensen EB (1987) The efficiency of systematic sampling in stereology and its prediction. *Journal of Microscopy* **147**, 229–263.

He J, Levine WS, Loeb GE (1991) Feedback gains for correcting small perturbations to standing posture. *IEEE Transactions on Automatic Control* **36**, 322–332.

Ikai M, Fukunaga T (1968) A study on training effect on strength per unit cross-sectional area of human muscle by means of ultrasonic measurement. *Internationale Zeitschrift für angewandte Physiologie und einschliesslich Arbeitphysiologie* **26**, 26–32.

Mayhew TM, Olsen DR (1991) Magnetic resonance imaging (MRI) and model-free estimates of brain volume determined using the Cavalieri principle. *Journal of Anatomy* **178**, 133–144.

Maughan RJ, Watson JS, Weir J (1983) Strength and cross-sectional area of human skeletal muscle. *Journal of Physiology* **338**, 37–49.

Méndez J, Keys A (1960) Density and composition of mammalian muscle. *Metabolism* **9**, 184–188.

Otten E (1988) Concepts and models of functional architecture in skeletal muscle. *Exercise and Sport Sciences Reviews* **16**, 89–137.

Pandy MG, Zajac FE (1991) Optimal muscular coordination strategies for jumping. *Journal of Biomechanics* **24**, 1–10.

Reid JG, Costigan PA (1987) Trunk muscle balance and muscular force. *Spine* **12**, 783–786.

Rugg SG, Gregor RJ, Mandelbaum BR, Chiu L (1990) In vivo moment arm calculations at the ankle using magnetic resonance imaging (MRI). *Journal of Biomechanics* **23**, 494–501.

Scott SH, Winter DA (1990) Internal forces at chronic running

injury sites. *Medicine and Science in Sports and Exercise* **22**, 357–369.

SCOTT SH, WINTER DA (1991) Technical note: comparison of three muscle pennation assumptions and their effect on isometric and isotonic force. *Journal of Biomechanics* **24**, 163–167.

SEIREG A, ARVIKAR RJ (1973) A mathematical model for evaluation of forces in lower extremities of the musculo-skeletal system. *Journal of Biomechanics* **6**, 313–326.

SPOOR CW, VAN LEEUWEN JL (1992) Technical note: knee muscle moment arms from MRI and from tendon travel. *Journal of Biomechanics* **25**, 201–206.

WICKIEWICZ TL, ROY RR, POWELL PL, EDGERTON VR (1983) Muscle architecture of the human lower limb. *Clinical Orthopaedics and Related Research* **178**, 275–283.

WOITTIEZ RD, HUIJING PA, BOOM HBK, ROZENDAL RH (1984) A three-dimensional muscle model: a quantified relation between form and function of skeletal muscles. *Journal of Morphology* **182**, 95–113.

APPENDIX

Derivation of fascicle orientation from sagittal and frontal projections

The 3D orientation of a fascicle can be computed mathematically given its projection in any 2 orthogonal planes. To begin, the orientation of a fascicle, d, oriented in 3D space is described by 2 angles: δ, the fascicle angle relative to the horizontal plane and θ, the fascicle angle relative to the frontal plane (Fig. 2). Let the angle of its projection in the frontal and sagittal planes relative to the horizontal plane be ϕ and σ, respectively. Some geometrical relationships of this fascicle and these projections include

$$d_b = d\cos\delta; \quad f_b = f\cos\phi; \quad s_b = s\cos\sigma, \tag{5}$$

$$d_h = d\sin\delta; \quad f_h = f\sin\phi; \quad s_h = s\sin\sigma, \tag{6}$$

$$f_b = d_b\cos\theta; \quad s_b = d_b\sin\theta, \tag{7}$$

$$d_h = f_h = s_h. \tag{8}$$

From equation 8, d_h and f_h can be substituted using equations 6, 5 and 7 to give,

$$\tan^2\delta = \cos^2\theta\tan^2\phi. \tag{9}$$

In a similar manner, d_h and s_h can be substituted to give

$$\tan^2\delta = \sin^2\theta\tan^2\sigma. \tag{10}$$

From pythagorean relations, equation 9 becomes

$$\tan^2\delta = (1-\sin^2\theta)\tan^2\phi. \tag{11}$$

Rearrangement of equation 11 to solve for $\sin^2\theta$, substitution of $\sin^2\theta$ into equation 10 and rearrangement to solve for δ gives,

$$\delta = \tan^{-1}\sqrt{\left(\frac{\tan^2\sigma\tan^2\phi}{\tan^2\sigma+\tan^2\phi}\right)}. \tag{12}$$

From equation 10

$$\theta = \sin^{-1}\left(\frac{\tan\delta}{\tan\sigma}\right). \tag{13}$$

Derivation of the projection in an oblique plane

For a projection plane perpendicular to the horizontal plane and at an angle β from the frontal plane, let the projection of a fascicle in this oblique plane be at an angle γ from the horizontal plane. Following equations 5–9 for this projection gives

$$\tan^2\delta = \cos^2(\theta-\beta)\tan^2\gamma \tag{14}$$

and by rearrangement

$$\gamma = \tan^{-1}\left(\frac{\tan\delta}{\cos(\theta-\beta)}\right). \tag{15}$$